Quaternary Geochronology 23 (2014) 1–8

Contents lists available at ScienceDirect

Quaternary Geochronology

journal homepage: www.elsevier.com/locate/quageo

Short communication

Pyroxene separation by HF leaching and its impact on helium surface-exposure dating

Gordon R.M. Bromley [a,b,*], Gisela Winckler [a], Joerg M. Schaefer [a], Michael R. Kaplan [a], Kathy J. Licht [c], Brenda L. Hall [b]

[a] Lamont-Doherty Earth Observatory, 61 Route 9W, Palisades, NY 10964, USA
[b] School of Earth & Climate Sciences/Climate Change Institute, Bryand Global Sciences Center, University of Maine, Orono, ME 04469, USA
[c] Department of Earth Sciences, Indiana University–Purdue University Indianapolis, 723 W. Michigan Street, Indianapolis, IN 46202, USA

ARTICLE INFO

Article history:
Received 6 February 2014
Received in revised form
9 April 2014
Accepted 15 April 2014
Available online 5 May 2014

Keywords:
Pyroxene
Cosmogenic helium
Surface-exposure dating
Acid leaching

ABSTRACT

Cosmogenic ^{3}He surface-exposure dating has become an important tool in earth surface sciences. Pyroxene, together with olivine, is the principal mineral phase for this technique, making ^{3}He particularly appropriate for volcanic lithologies. However, two important factors that affect the viability of the method are the extensive, thus expensive, preparation procedure and the often under-constrained purity of pyroxene separates. Here, we present an approach to preparing pyroxenes for ^{3}He dating, adapted from the quartz-separation method for ^{10}Be and ^{26}Al analyses, which utilises hydrofluoric-acid leaching to improve pyroxene purity and streamline the pyroxene separation procedure. In addition to producing abundant sample in relatively little time, the results of two experiments demonstrate that acid leaching (i) yields samples of higher purity than conventional methods, reflected in slightly elevated ^{3}He concentrations, and (ii) reduces ^{4}He concentrations, in turn elevating the ^{3}He/^{4}He ratio. This new protocol for preparing pyroxenes thus has the potential to increase the precision and accuracy of cosmogenic ^{3}He surface-exposure dating.

1. Introduction

The suitability of cosmogenic ^{3}He for geochronologic applications lies in its high and well-constrained production rate (e.g., Kurz, 1986a, 1986b; Cerling, 1990; Lal, 1991; Cerling and Craig, 1994; Licciardi et al., 1999; Dunai and Wijbrans, 2000; Gayer et al., 2004; Amidon et al., 2008; Amidon and Farley, 2010; Goehring et al., 2010; Blard et al., 2013), the low detection limit of helium, and the effective retention of helium in common mineral phases, such as pyroxene, olivine, zircon, and garnet, as well as Fe–Ti oxides (Gosse and Phillips, 2001; Bryce and Farley, 2002; Gayer et al., 2004; Kober et al., 2005; Amidon et al., 2008; Amidon and Farley, 2010). Since helium is stable and has a low detection limit/production rate ratio, this method potentially can be used to date surfaces ranging in age from centuries (Kurz and Geist, 1999; Blard et al., 2006a) to millions of years (e.g., Bruno et al., 1997; Schäfer et al., 1999, 2000; Dunai et al., 2005; Van der Wateren et al., 1999). Owing to the relatively straightforward sample-preparation process, and because helium can be measured on commercial sector-field noble gas mass spectrometers, cosmogenic ^{3}He surface-exposure dating also is more economical than other, costlier methods relying on accelerator mass spectrometry (such as ^{10}Be and ^{26}Al) and can be performed *in house* in noble–gas mass spectrometry laboratories.

Cosmogenic ^{3}He ($^{3}He_{cos}$) is produced in the mineral lattice primarily through spallation reactions, with lesser amounts derived from thermal-neutron capture on ^{6}Li (Dunai et al., 2007). ^{4}He also is produced cosmogenically, but in concentrations that are negligible compared to other sources. Magmatic helium (He_{mag}), derived from the mantle, is concentrated in fluid and gas inclusions within the phenocrysts and can constitute a major source of both isotopes (Kurz, 1986b). Radiogenic ^{4}He ($^{4}He_{rad}$), meanwhile, is produced in both pyroxenes and the parent rock via U/Th-decay and ^{4}He implantation from small mineral inclusions or accessory minerals (such as zircons or monzanite) attached to the pyroxenes and olivines (Kurz and Brook, 1994; Farley et al., 1996; Gosse and Phillips, 2001; Blard et al., 2006a). This same process also generates small amounts of ^{3}He through interactions with matrix-sited ^{6}Li (Andrews and Kay, 1982). Each of these sources of helium must be accounted for – and, if necessary, corrected for – in order to make accurate surface-exposure age determinations

* Corresponding author. School of Earth & Climate Sciences/Climate Change Institute, Bryand Global Sciences Center, University of Maine, Orono, ME 04469, USA.
E-mail address: gordon.r.bromley1@maine.edu (G.R.M. Bromley).

http://dx.doi.org/10.1016/j.quageo.2014.04.003
1871-1014/

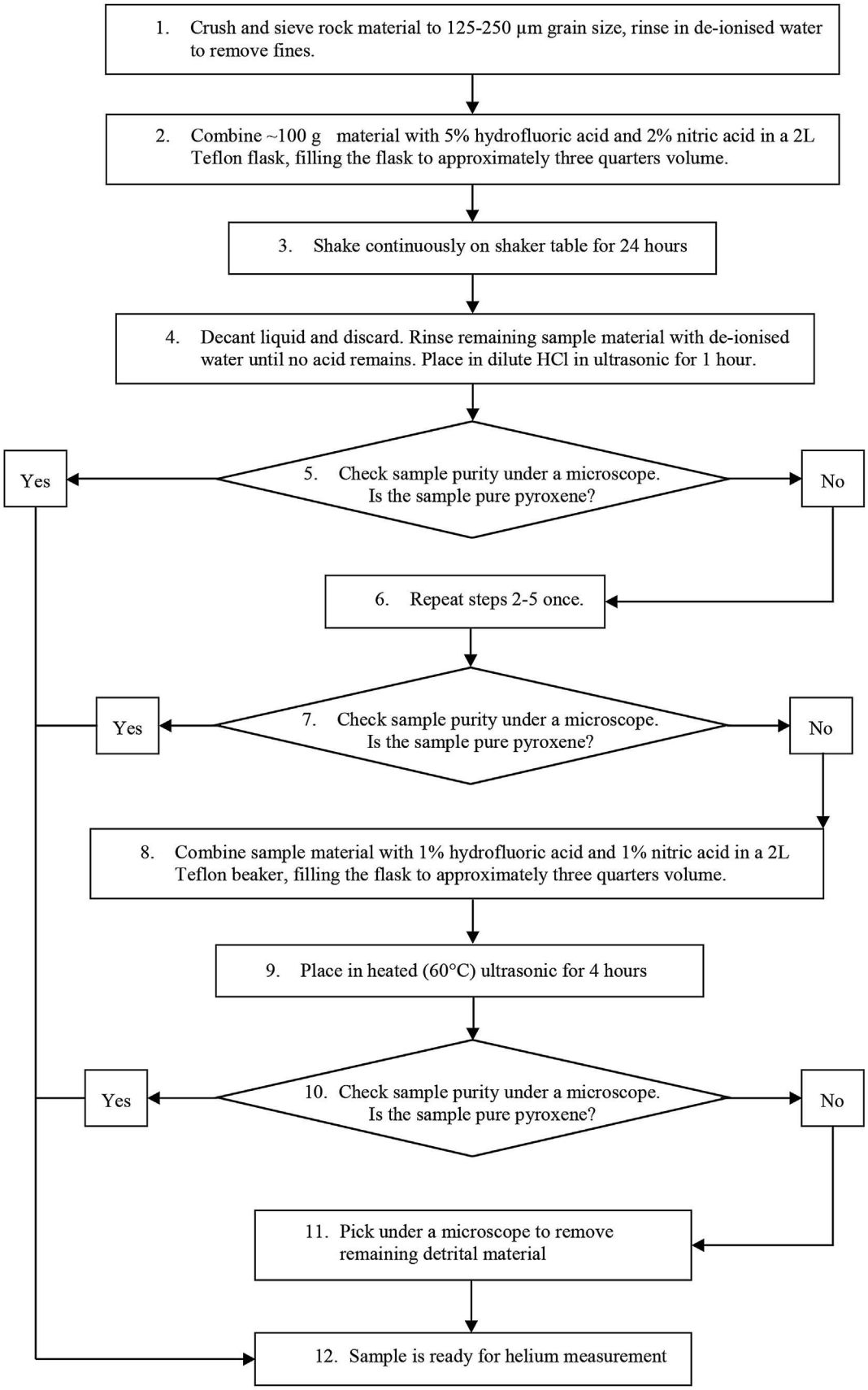

Fig. 1. Schematic diagram detailing the acid-leaching procedure for separating pyroxene. 'Pure pyroxene' refers to samples in which, upon checking under a microscope, no foreign material is observed.

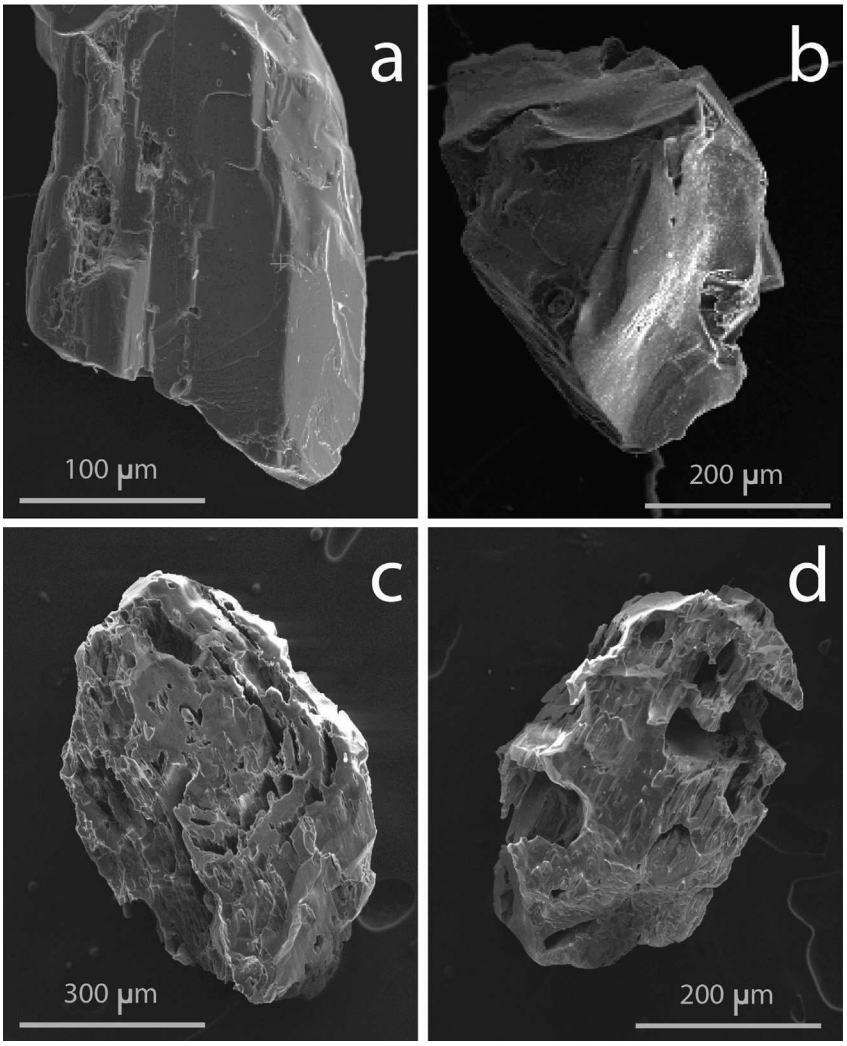

Fig. 2. Electron-microscope images of non-leached (a, b) and leached (c, d) pyroxene from Coropuna andesite (sample COR-09-08), highlighting the physical effects of hydrofluoric acid on pyroxene.

(Blard et al., 2006b). Ideally, non-cosmogenic helium concentrations in samples are low.

To account for the presence in pyroxene and olivine of non-cosmogenic helium, a two-phased approach was devised by Kurz (1986a) in which samples first are crushed in vacuum and then fused. Crushing preferentially releases magmatic helium trapped in fluid inclusions, allowing the $^3He/^4He_{mag}$ ratio to be measured. Subsequent fusion of the crushed material releases any remaining helium, reportedly a combination of both magmatic and cosmogenic components. Using the equation

$$^3He_{cos} = {}^3He_{total} - [(^3He/^4He_{mag}) * {}^4He_{total}]$$

where $^3He_{cos}$ is the concentration of cosmogenic helium, $^3He_{total}$ and $^4He_{total}$ are concentrations of those isotopes released by fusion, and $^3He/^4He_{mag}$ is the magmatic ratio acquired by crushing, the concentration of $^3He_{cos}$ in a sample is determined (Kurz, 1986a). A key assumption in this widely – and successfully – used approach is that all ^4He in a sample is magmatic (i.e., $^4He_{total} = {}^4He_{mag}$). In a recent study, however, Blard and Farley (2008) suggested that thorough consideration of non-cosmogenic helium is not yet standard practise in ^3He surface-exposure applications and highlighted the potential impact of $^4He_{rad}$ on geochronologic applications. As a product of U/Th decay, $^4He_{rad}$ is generated both within pyroxene grains and in the surrounding groundmass. Additionally, the long stopping distance ($\sim$20 μm) of α-particles in these minerals results in exchange between host and phenocryst and can lead to relative helium enrichment (or depletion) of these outermost layers. Blard and Farley (2008) concluded that, if $^4He_{rad}$ constitutes a significant portion of the total ^4He in a sample, failure to account for this radiogenic component will result in over-correcting for the effects of $^3He_{mag}$ (Blard and Farley, 2008). Accordingly, those authors presented a method by which $^4He_{rad}$ concentrations within both mineral grains and in the surrounding groundmass could be estimated.

Motivated by that study, we address an additional source of uncertainty: the purity of pyroxene separates. Following standard preparation procedures for ^3He dating (see Section 2), pyroxene separation typically is finalised by hand-picking (e.g., Kurz, 1986b; Brook et al., 1995; Bruno et al., 1997; Licciardi et al., 1999; Schäfer et al., 1999; Blard et al., 2009) and hence the resulting purity is subjective and difficult to report, though typically 100% pyroxene purity is assumed in the ^3He age calculations. However, this approach risks the incorporation of non-helium-retentive impurities (e.g., feldspar, groundmass, accessory minerals) that potentially could lead to over-estimation of sample weight and thus

Fig. 3. Map showing the locations of Nevado Coropuna, Peru, and Mount Howe, Transantarctic Mountains.

underestimation of measured ^{3}He concentrations. Moreover, elemental analysis frequently is conducted for pure pyroxenes but cannot account for contributions by minor amounts of such impurities. Here, we describe a simple but rigorous chemical procedure for producing clean pyroxene separates. We make the case that this new pyroxene separation procedure increases the purity of pyroxene separates and makes the separation more objective, cuts dramatically the amount of time spent 'hand-picking' samples, and reduces the $^{4}He_{rad}$ background. The presented approach also results in greater yields of pure pyroxene in less time than the traditional hand-picking method. We discuss the implications of this procedure for improving the cosmogenic ^{3}He dating technique. Owing to its ready dissolution in hydrofluoric acid, we note that the approach described here is not applicable to olivines.

2. Methods

2.1. Hydrofluoric preparation of pyroxenes for ^{3}He measurement

The conventional approach to preparing both pyroxenes and olivines for helium isotope measurements exploits the high density and magnetic characteristics of these minerals and uses predominantly mechanical means (e.g., Kurz and Brook, 1994; Schäfer et al., 1999). Here, we describe a revised protocol for separating pyroxene from andesite and dolerite that is an adaptation of the quartz separation procedure for ^{10}Be and ^{26}Al analysis presented originally by Kohl and Nishiizumi (1992). To demonstrate the efficacy of this approach, we used pyroxenes derived from two very different lithologies: Peruvian andesite and Ferrar dolerite from Antarctica. Andesite samples were collected from Nevado Coropuna (15°33′S, 72°93′W), a Quaternary stratovolcano located in the southern Peruvian Andes (Fig. 3). Coropuna andesite is characterised by phenocrysts of pyroxene (augite), plagioclase, titanomagnetite, amphibole, and biotite set in a hyalopilitic groundmass (Venturelli et al., 1978) and has been used effectively in two recent ^{3}He surface-

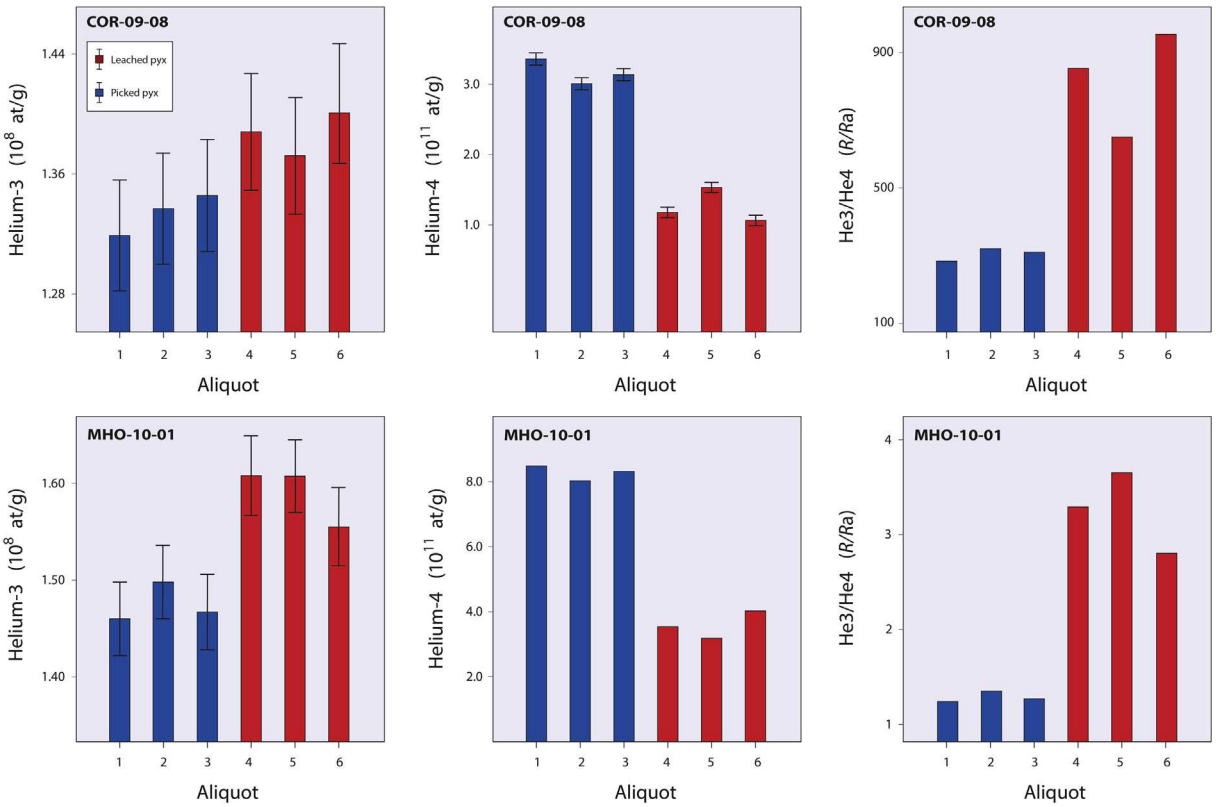

Fig. 4. Comparison of helium concentrations (atoms/g) and ^{3}He/^{4}He ratios for non-leached (blue) and leached (red) aliquots, with 1 σ uncertainty. ^{3}He/^{4}He ratios are given relative to the atmospheric ^{3}He/^{4}He value $Ra = 1.384 \times 10^{-6}$. (For interpretation of the references to colour in this figure legend, the reader is referred to the web version of this article.)

exposure studies (Bromley et al., 2009, 2011). Samples of Ferrar dolerite (formation age ~177 Ma; Fleming et al., 1997) were collected from Mt. Howe (87°22′S, 149°30′W), Antarctica (Fig. 3). While this lithology has been used extensively in Antarctic ^{3}He surface-exposure studies (e.g., Bruno et al., 1997; Ackert and Kurz, 2004; Margerison et al., 2005), Ferrar dolerite can be problematic to separate due to small mineral-size and considerable intergrowth with minerals such as plagioclase and hornblende (Schäfer et al., 1999).

Following the initial crushing steps described in Schäfer et al. (1999), the 125–250 μm whole-rock fraction is leached in a hydrofluoric-nitric acid cocktail to remove the majority of non-pyroxene minerals as well as the outer layers of the pyroxene grains. Fig. 1 shows a flow diagram of the individual separation steps. Specifically, ~100 g of whole rock is combined with 5% HF: 2% HNO_3 in a 2-litre Teflon flask and placed on a shaker table for 24 h. While this treatment can be sufficient to dissolve all but the pyroxenes, any remaining non-pyroxene material is removed by repeating the process. Leached samples are rinsed in deionised water and oven-dried at 50 °C, whereupon they are inspected visually under a binocular microscope. For both lithologies investigated, leaching results in significantly larger yields of pyroxene (averaging 5 g) in less time than the traditional method.

If necessary – for example, when the pyroxene concentration in a rock is relatively low – the crushed rock can be passed through a heavy liquid step to remove lighter minerals prior to the HF-leaching. Occasionally, fluorites form on the surfaces of pyroxenes during the HF-leaching process. These precipitates can be removed by leaching samples in 6 M HCl on a shaker table (or unheated ultrasonic bath) for ~1 h. Visibly, the pyroxenes show evidence of acid corrosion removing the outer pyroxene layers (Fig. 2), the degree of which depends on the duration of leaching. In extreme cases (e.g., three leaching periods), grains are riddled with holes and have a structure akin to Swiss cheese (Ivy-Ochs et al., 1998). Mineral surfaces are shiny, with no trace of adhering groundmass. We present two experiments to test the effects, if any, of the new pyroxene separation protocol (Fig. 1) on helium isotope concentrations. Experiment 1 uses pyroxenes from the Coropuna andesite and Ferrar Dolerite and compares leached versus traditionally separated pyroxenes from these samples. Experiment 2 assesses the effects of progressively more aggressive leaching on pyroxenes from the Coropuna andesite.

2.2. Experiment 1: helium concentrations in pyroxene from Coropuna andesites and Ferrar Dolerites: leached vs. non-leached aliquots

We compared helium concentrations in three multiple aliquots of leached and non-leached pyroxenes from two samples: COR-09-08 (andesite) from Nevado Coropuna and MHO-11-01 (dolerite) from Mt. Howe. Non-leached aliquots of each sample were prepared following the conventional methodology described above (blue bars in Fig. 4). Leached pyroxene separates were prepared as shown in Fig. 1 (red bars in Fig. 4). Helium measurements were made on the same day to minimise the effects of mass-spectrometer variability on analyses. Because this experiment expressly was designed to assess the effects of leaching on helium concentrations, we did not perform in vaccuo crushing on any samples.

In both lithologies, leaching has a notable impact on helium isotope concentrations. First, ^{3}He concentrations are slightly higher (~6%) in leached pyroxenes than in non-leached pyroxenes (Fig. 4; Table 1), both for andesite and dolerite samples. Second, ^{4}He concentrations in the leached pyroxene are less than half those of non-leached pyroxenes. In both andesitic and doleritic lithologies, average ^{4}He concentrations are ~60% lower (Fig. 4; Table 1). Correspondingly, ^{3}He/^{4}He ratios are much higher in both sets of leached aliquots than in those prepared traditionally. Table 2 compares helium concentrations from seven additional pyroxenes separates, leached versus picked, from andesites collected from Nevado Coropuna as part of a separate glacial-chronologic investigation. As this dataset illustrates, leaching routinely yields higher ^{3}He concentrations than aliquots of the same samples prepared in the traditional manner (Fig. 5). While the magnitude of this offset is variable, owing to the differing amounts of groundmass removed by leaching, we observed a mean increase of 5% (±2%) in the concentration of ^{3}He concentration due to leaching (Fig. 5, Table 2). Because the non-cosmogenic ^{3}He contributions are negligible in these samples (see Bromley et al., 2009, 2011), this effect translates linearly into an increase of the ^{3}He exposure age.

2.3. Experiment 2: effects of progressive leaching on helium concentrations

We prepared four ~100 mg aliquots of a single sample (COR-10-04) of Peruvian andesite (Table 3, Fig. 6). Aliquot 1 was prepared

Table 1
Sample details and helium isotope data for leached and non-leached pyroxene separated from andesite and Ferrar Dolerite, as described in Experiment 1. ^{3}He/^{4}He ratios are given as measured and relative to the atmospheric ^{3}He/^{4}He value $Ra = 1.384 \times 10^{-6}$.

Sample number	Type	^{3}He (at./g)	1 σ (at./g)	^{4}He (at./g)	1 σ (at./g)	^{3}He/^{4}He	1 σ	^{3}He/^{4}He (R/R_a)
COR-09-08								
Aliquot 1	Non-leached	1.32×10^8	3.74×10^6	3.36×10^{11}	8.61×10^9	3.93×10^{-4}	1.5×10^{-5}	284
Aliquot 2	Non-leached	1.34×10^8	3.76×10^6	3.01×10^{11}	7.74×10^9	4.44×10^{-4}	1.69×10^{-5}	321
Aliquot 3	Non-leached	1.35×10^8	3.73×10^6	3.14×10^{11}	7.88×10^9	4.29×10^{-4}	1.61×10^{-5}	310
Mean	Non-leached	1.34×10^8	3.74×10^6	3.17×10^{11}	8.08×10^9	4.22×10^{-4}	1.6×10^{-5}	305
Aliquot 4	Leached	1.39×10^8	3.92×10^6	1.18×10^{11}	7.61×10^9	1.18×10^{-3}	8.32×10^{-5}	853
Aliquot 5	Leached	1.37×10^8	3.88×10^6	1.52×10^{11}	7.38×10^9	9.02×10^{-4}	5.06×10^{-5}	652
Aliquot 6	Leached	1.41×10^8	3.98×10^6	1.06×10^{11}	7.47×10^9	1.32×10^{-3}	1.0×10^{-4}	954
Mean	Leached	1.39×10^8	3.93×10^6	1.25×10^{11}	7.49×10^9	1.13×10^{-3}	7.79×10^{-5}	820
MHO-10-01								
Aliquot 1	Non-leached	1.46×10^8	3.81×10^6	8.48×10^{13}	1.91×10^{11}	1.72×10^{-6}	4.51×10^{-8}	1.2
Aliquot 2	Non-leached	1.5×10^8	3.81×10^6	8.03×10^{13}	1.72×10^{11}	1.87×10^{-6}	4.76×10^{-8}	1.4
Aliquot 3	Non-leached	1.47×10^8	3.89×10^6	8.32×10^{13}	2.17×10^{11}	1.76×10^{-6}	4.69×10^{-8}	1.3
Mean	Non-leached	1.48×10^8	3.84×10^6	8.28×10^{13}	1.93×10^{11}	1.93×10^{-6}	4.65×10^{-8}	1.3
Aliquot 4	Leached	1.61×10^8	3.9×10^6	3.54×10^{13}	4.54×10^{10}	4.55×10^{-6}	1.1×10^{-7}	3.3
Aliquot 5	Leached	1.61×10^8	3.84×10^6	3.18×10^{13}	4.17×10^{10}	5.05×10^{-6}	1.21×10^{-7}	3.7
Aliquot 6	Leached	1.56×10^8	3.82×10^6	4.02×10^{13}	5.12×10^{10}	3.87×10^{-6}	9.52×10^{-8}	2.8
Mean	Leached	1.59×10^8	3.85×10^6	3.58×10^{13}	4.61×10^{10}	4.49×10^{-6}	1.09×10^{-7}	3.3

Table 2
Sample details and helium isotope data for the seven additional paired leached–non-leached pyroxenes separated from andesites from Nevado Coropuna. Also shown are relative differences (Δ%) in ^{3}He and ^{4}He between leached and non-leached aliquots. All samples are from the surfaces of glacial erratic boulders.

Sample number	^{3}He Picked (at./g)	1σ (at./g)	^{4}He Picked (at./g)	1σ (at./g)	^{3}He/^{4}He Picked	1σ	^{3}He Leached (at./g)	1σ (at./g)	^{4}He Leached (at./g)	1σ (at./g)	^{3}He/^{4}He Leached	1σ	^{3}He Δ%	^{4}He Δ%
COR-06-13	1.86×10^7	4.35×10^5	1.19×10^{12}	2.23×10^{10}	1.57×10^{-5}	4.73×10^{-7}	1.92×10^7	2.02×10^5	4.37×10^{11}	4.60×10^9	4.39×10^{-5}	1.39×10^{-6}	3.1	−63
COR-06-16	1.49×10^7	3.59×10^5	1.11×10^{12}	1.91×10^{10}	1.34×10^{-5}	3.98×10^{-7}	1.6×10^7	1.66×10^5	5.56×10^{11}	5.77×10^9	2.88×10^{-5}	1.12×10^{-6}	6.9	−50
COR-09-08	1.31×10^8	1.29×10^6	3.27×10^{11}	2.44×10^9	4.0×10^{-4}	4.95×10^{-6}	1.33×10^8	1.22×10^6	2.06×10^{11}	1.07×10^7	6.42×10^{-4}	5.9×10^{-6}	1.3	−37
COR-09-09	2.84×10^7	7.12×10^5	1.04×10^{12}	1.42×10^{10}	2.73×10^{-5}	7.79×10^{-7}	2.91×10^7	4.32×10^5	1.56×10^{11}	1.84×10^9	1.87×10^{-4}	3.55×10^{-6}	2.5	−85
COR-10-08	6.85×10^7	9.03×10^5	3.93×10^{11}	3.12×10^9	1.74×10^{-4}	2.68×10^{-6}	7.33×10^7	1.25×10^5	2.9×10^{11}	5.78×10^9	2.53×10^{-4}	6.64×10^{-6}	6.5	−26
COR-10-91	1.92×10^7	5.53×10^5	8.47×10^{10}	4.34×10^9	2.26×10^{-4}	1.33×10^{-5}	2.06×10^7	4.74×10^5	6.19×10^{10}	2.74×10^9	3.32×10^{-4}	1.66×10^{-5}	7	−27
COR-10-92	1.98×10^7	4.83×10^5	1.10×10^{11}	3.48×10^9	1.8×10^{-4}	7.21×10^{-6}	2.11×10^7	4.26×10^5	8.19×10^{10}	2.39×10^9	2.58×10^{-4}	9.16×10^{-6}	6.3	−25

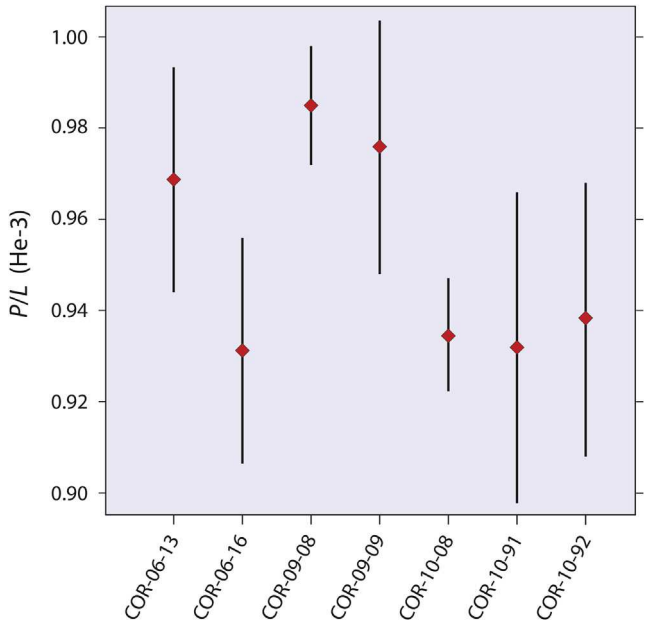

Fig. 5. Helium-3 ratios for the seven non-leached/leached pairs from Nevado Coropuna listed in Table 2, given as the ratio of ^{3}He concentration in non-leached (P) to leached (L) aliquots with 1 σ uncertainty.

following the traditional non-leaching protocol; , Aliquots 2 and 3 were leached in 5% HF: 2% HNO_3 on the shaker table for one and two 24-h periods, respectively; and Aliquot 4 was prepared as Aliquot 3, with the additional step of a 4-hour leaching in 1% HF: 1% HNO_3 in a heated (60 °C) ultrasonic bath. Leached samples were checked under a microscope for any foreign grains prior to helium measurement.

Among the four aliquots measured, we note that the mean ^{3}He concentrations in the three leached aliquots are 9% (±4%) higher than that of the picked aliquot (Aliquot 1) (Fig. 6; Table 3). Together, these data indicate that ^{3}He is not being lost even during prolonged pyroxene leaching and slight heating. In contrast, ^{4}He concentrations are on average lower 21% (±13%) in each of the leached pyroxenes than in the non-leached aliquot (Fig. 6, Table 3), a pattern that in general is consistent with Experiment 1. However, although this decrease in ^{4}He is not linear, we note that the most substantial decrease in ^{4}He is related to the final, most aggressive, leaching/heating step exclusive to Aliquot 4.

3. Discussion

Our data demonstrate that more rigorous (and objective) pyroxene separation techniques can improve measurements of cosmogenic helium. Relative to non-leached samples, the leaching experiments described here resulted in slightly (7 ± 3%) increased ^{3}He and (46 ± 22%) considerably lower ^{4}He concentrations for most aliquots. We attribute the elevated ^{3}He to increased sample purity, since leaching removes adhering, non-helium-bearing minerals and groundmass that otherwise would dilute the signal-to-weight ratio. Moreover, we note that the observed increase in ^{3}He was greater in the Antarctic sample than in the Peruvian pyroxene (Fig. 4), suggesting that different lithologies may be more prone to adhering impurities. Leaching would also remove any adhering minerals that could themselves contain significant (and variable) concentrations of helium, such as magnetite. There is no evidence for ^{3}He loss from pyroxene even during extreme leaching (Table 3).

The considerable decrease in ^{4}He in the leached pyroxene likely reflects removal of the outer few microns of the phenocrysts by the

Table 3
Sample details and helium isotope data for non-leached and progressively leached pyroxenes as described in Experiment 2. [ST] and [US] denote shaker table and ultrasonic, respectively. $^3He/^4He$ ratios are given as measured and relative to the atmospheric $^3He/^4He$ value $Ra = 1.384 \times 10^{-6}$.

Sample number	Type	^3He (at./g)	1 σ (at./g)	^4He (at./g)	1 σ (at./g)	$^3He/^4He$	1 σ	$^3He/^4He$ (R/R_a)
COR-10-04								
Aliquot 1	Non-leached	3.29×10^7	6.25×10^5	4.49×10^{11}	4.09×10^9	7.32×10^{-5}	1.54×10^{-6}	53
Aliquot 2	24-hr HF/HNO_3 [ST]	3.74×10^7	1.23×10^6	3.8×10^{11}	7.16×10^9	9.85×10^{-5}	3.75×10^{-6}	71
Aliquot 3	48-hr HF/HNO_3 [ST]	3.45×10^7	1.34×10^6	4.01×10^{11}	9.68×10^9	8.62×10^{-5}	3.95×10^{-6}	62
Aliquot 4	48-hr HF/HNO_3 [ST] & 4-hr HF/HNO_3 [US]	3.69×10^7	1.23×10^6	2.88×10^{11}	6.41×10^9	1.28×10^{-4}	5.13×10^{-6}	92

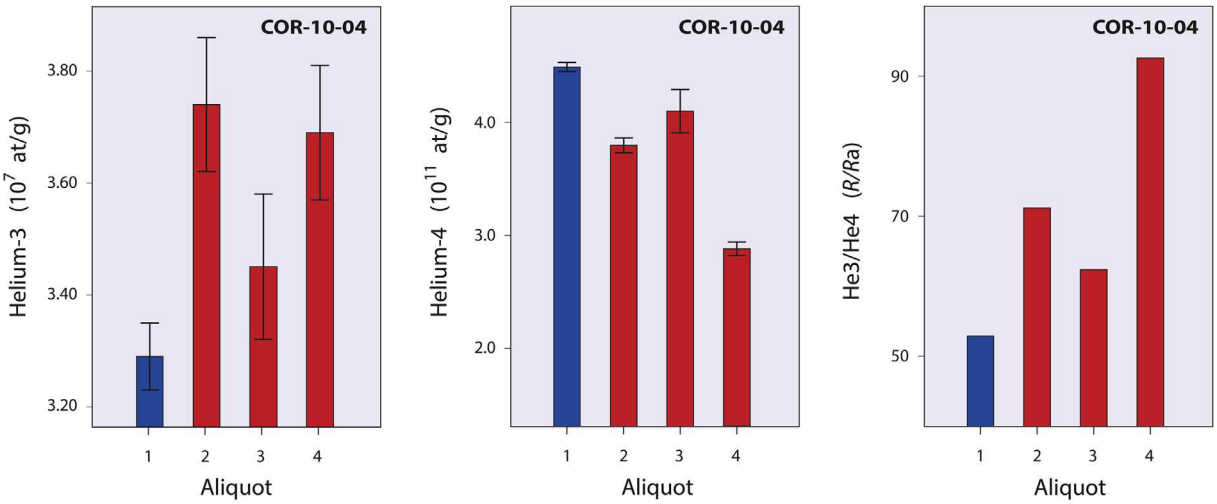

Fig. 6. Helium concentrations (atoms/g) and $^3He/^4He$ ratios for non-leached (blue) and progressively leached (red) aliquots, with 1 σ uncertainty. $^3He/^4He$ ratios are given relative to the atmospheric $^3He/^4He$ value $Ra = 1.384 \times 10^{-6}$. (For interpretation of the references to colour in this figure legend, the reader is referred to the web version of this article.)

leaching process. Visual inspection of leached grains revealed significant acid corrosion of the mineral surface (Fig. 2). Since penetration depth of alpha-particles/^4He nuclei implanted by U/Th decay of accessory minerals is on the order of ~20 μm (Farley et al., 2006; Min et al., 2006; Blard and Farley, 2008), removal of exterior micrometers of the pyroxene grains by the leaching process could explain the reduction of the radiogenic helium component. This concept is not a new one: (U–Th)/He investigations routinely employ chemical or physical means to remove these $^4He_{rad}$–enriched outer layers (e.g., Farley, 2002; Aciego et al., 2007; Blackburn et al., 2007).

These results have compelling implications for ^3He surface-exposure dating. First, increased ^3He concentrations due to cleaner pyroxene produced by the HF-leaching protocol improve the precision of ^3He exposure-age calculations. As shown in Table 2, surface-exposure samples consisting of leached pyroxenes contain as much as 7% more ^3He than their non-leached counterparts. Second, the large reduction in ^4He in both andesitic and doleritic phenocrysts indicates that the radiogenic inventory of the outer rims of pyroxene grains can be considerable even in relatively young (<2 Ma) rocks. If one assumes all measured ^4He to be magmatic in origin (e.g., Kurz, 1986b; Brook et al., 1995; Licciardi et al., 2001), the 'corrected' surface-exposure ages will be erroneously young, as pointed out by Blard and Farley (2008). Moreover, this approach might compromise the internal consistency of a dataset, since concentrations of $^4He_{rad}$ – and thus the magnitude of any magmatic correction – can vary among samples. Thus, our findings support the argument that $^4He_{rad}$ concentrations need to be accounted for in order to correct effectively for magmatic helium. This goal can be achieved either through physical removal of the outer few microns (e.g., Aciego et al., 2007; this study) and estimation of internally produced $^4He_{rad}$ (Blard and Farley, 2008) or via estimation of both implanted and internal helium components (Blard and Farley, 2008), followed by the standard *in vacuo* crushing procedure to measure magmatic helium (Kurz, 1986b).

We introduce a simple yet robust HF-leaching step for the separation of pyroxenes from various rock types for cosmogenic ^3He dating. This methodology has the potential to (i) streamline the pyroxene preparation process, thereby producing larger yields of pure pyroxene in less time than the traditional method, (ii) remove the 'diluting' effects of non-pyroxene material that might otherwise escape visual detection, and (iii) reduce the radiogenic helium background in samples from both young and old formations.

Acknowledgements

This work was supported by NSF Grants EAR-10-03427, ANT-0944475, and PLR-1043589, and is part of the Lamont-Doherty Earth Observatory postdoctoral fellowship of G. Bromley. We thank Roseanne Schwartz, Linda Baker, and Karin Needleman for their help during sample processing and analyses. We are particularly grateful to P.-H. Blard and an anonymous reviewer whose comments greatly improved an earlier version of this manuscript. This is LDEO contribution. This is LDEO contribution #7788.

Editorial handling by: Didier Bourles

References

Aciego, S.M., DePaolo, D.J., Kennedy, B.M., Lamb, M.P., Sims, K.W.W., Dietrich, W.E., 2007. Combining [^3He] cosmogenic dating with U–Th/He eruption ages using olivine in basalt. Earth Planet. Sci. Lett. 254, 288–302.

Ackert, R.D., Kurz, M.D., 2004. Age and uplift rates of Sirius group sediments in the Dominion Range, Antarctica, from surface exposure dating and geomorphology. Glob. Plane. Change 42, 207–225.
Amidon, W.H., Farley, K.A., 2010. Cosmogenic 3He production rates in apatite, zircon and pyroxene inferred from Bonneville flood erosional surfaces. Quat. Geo. 6, 10–21.
Amidon, W.H., Farley, K.A., Burbank, D.W., Pratt-Sitaula, B., 2008. Anomalous cosmogenic 3He production and elevation scaling in the high Himalaya. Earth Planet. Sci. Lett. 265, 287–301.
Andrews, J.N., Kay, R.L.F., 1982. Natural production of tritium in permeable rocks. Nature 298, 361–363.
Blackburn, T.J., Stockli, D.F., Walker, J.D., 2007. Magnetite (U-Th)/He dating and its application to the geochronology of intermediate to mafic volcanic rocks. Earth Planet. Sci. Lett. 259, 360–371.
Blard, P.-H., Bourles, D., Lave, J., Pik, R., 2006a. Applications of ancient cosmic-ray exposures: theory, techniques and limitations. Quat. Geo. 1, 59–73.
Blard, P.-H., Pik, R., Lavé, J., Bourlès, D., Burnard, P.G., Yokochi, R., Marty, B., Trusdell, F., 2006b. Cosmogenic 3He production rates revisited from evidences of grain size dependent release of matrix sited helium. Earth Planet. Sci. Lett. 247, 222–234.
Blard, P.-H., Farley, K.A., 2008. The influence of radiogenic ^{4}He on cosmogenic ^{3}He determinations in volcanic olivine and pyroxene. Earth Planet. Sci. Lett. 276, 20–29.
Blard, P.-H., Lave, J., Farley, K.A., Fornari, M., Jiménez, J., Ramirez, V., 2009. Late local glacial maximum in the Central Altiplano triggered by cold and locally-wet conditions during the paleolake Tauca episode (17–15 ka, Heinrich 1). Quat. Sci. Rev. 28, 3414–3427.
Blard, P.-H., Lavé, J., Sylvestre, F., Placzek, C.J., Claude, C., Galy, V., Condom, T., Tibari, B., 2013. Cosmogenic ^{3}He production rate in the high tropical Andes (3800 m, 20°S): Implications for the local last glacial maximum. Earth Planet. Sci. Lett. 377–378, 260–275.
Bromley, G.R.M., Schaefer, J.M., Winckler, G., Hall, B.L., Todd, C.E., Rademaker, K.M., 2009. Relative timing of last glacial maximum and late-glacial events in the central tropical Andes. Quat. Sci. Rev. 28, 2514–2526.
Bromley, G.R.M., Hall, B.L., Schaefer, J.M., Winckler, G., Todd, C.E., Rademaker, K.M., 2011. Glacier fluctuations in the southern Peruvian Andes during the late-glacial period, constrained with cosmogenic ^{3}He. J. Quat. Sci. 26, 37–43.
Brook, E.J., Kurz, M.D., Ackert, R.P., Raisbeck, G., Yiou, F., 1995. Cosmogenic nuclide exposure ages and glacial history of late Quaternary Ross Sea drift in McMurdo Sound, Antarctica. Earth Planet. Sci. Lett. 131, 41–56.
Bruno, L.A., Baur, H., Graf, T., Schlüchter, C., Signer, P., Wieler, R., 1997. Dating of Sirius Group tillites in the Antarctic Dry Valleys with cosmogenic ^{3}He and ^{21}Ne. Earth Planet. Sci. Lett. 147, 37–54.
Bryce, J.G., Farley, K.A., 2002. ^{3}He exposure dating of magnetite. In: Podosec, F.A. (Ed.), Goldschmidt Conference, Geochimica et Cosmochimica Acta 66 p. A108.
Cerling, T.E., 1990. Dating geomorphologic surfaces using cosmogenic ^{3}He. Quat. Res. 33, 148–156.
Cerling, T.E., Craig, H., 1994. Geomorphology and in-situ cosmogenic isotopes. Ann. Rev. Earth Plan. Sci. 22, 273–317.
Dunai, T.J., Wijbrans, J.R., 2000. Long-term cosmogenic 3He production rates (152 ka–1.35Ma) from 40Ar/39Ar dated basalt !ows at 29°N latitude. Earth Plan. Sci. Lett. 176, 147–156.
Dunai, T.J., Gónzalez-López, G.A., Juez-Larré, J., 2005. Oligocene/Miocene age of aridity in the Atacama desert revealed by exposure dating of erosion sensitive landforms. Geology 33, 311–324.
Dunai, T.J., Stuart, F.M., Pik, R., Burnard, P., Gayer, E., 2007. Production of ^{3}He in crustal rocks by cosmogenic thermal neutrons. Earth Plan. Sci. Lett. 258, 228–236.
Farley, K.A., 2002. (U-Th)/He dating: techniques, calibrations, and applications. Rev. Mineral. Geochem. 47, 819–844.
Farley, K.A., Wolf, R.A., Silver, L.T., 1996. The effects of long alpha-stopping distances on (U-Th)/He ages. Geochim. Cosmochim. Acta 60, 4223–4229.
Farley, K.A., Libarkin, J., Mukhopadhyay, S., Amidon, W., 2006. Cosmogenic and nucleogenic 3He in apatite, titanite, and zircon. Earth Plan. Sci. Lett. 248, 451–461.
Fleming, T.H., Heimann, A., Foland, K.A., Elliot, D.H., 1997. ^{40}Ar/^{39}Ar geochronology of Ferrar Dolerite sills from the Transantarctic Mountains, Antarctica: Implications for the age and origin of the Ferrar magmatic province. Geol. Soc. Am. Bull. 109, 533–546.
Gayer, E., Pik, R., Lavé, J., France-Lanord, C., Bourlés, D., Marty, B., 2004. Cosmogenic 3He in Himalayan garnets indicating an altitude dependence of the 3He/10Be production ratio. Earth Plan. Sci. Lett. 229, 91–101.
Goehring, B.M., Kurz, M.D., Balco, G., Schaefer, J.M., Licciardi, J., Lifton, N., 2010. A reevaluation of *in situ* cosmogenic ^{3}He production rates. Quat. Geochron. 5, 410–418.
Gosse, J.C., Phillips, F.M., 2001. Terrestrial in situ cosmogenic nuclides: theory and application. Quat. Sci. Rev. 20, 1475–1560.
Ivy-Ochs, S., Kubik, P.W., Masarik, J., Wieler, R., Bruno, L., Schlüchter, C., 1998. Preliminary results on the use of pyroxene for 10Be surface exposure dating. Schweiz. Mineral. Petrogr. Mittl. 78, 375–382.
Kober, F., Ivy-Ochs, S., Leya, I., Baur, H., Magna, T., Wieler, R., Kubik, P.W., 2005. In situ cosmogenic 10Be and 21Ne in sanidine and in situ cosmogenic 3He in Fe–Ti-oxide minerals. Earth Plan. Sci. Lett. 236, 404–418.
Kohl, C.P., Nishiizumi, K., 1992. Chemical isolation of quartz for *in-situ*-produced cosmogenic nuclides. Geochim. Cosmochim. Acta 56, 3583–3587.
Kurz, M.D., 1986a. Cosmogenic helium in a terrestrial igneous rock. Nature 320, 435–439.
Kurz, M.D., 1986b. In situ production of terrestrial cosmogenic helium and some applications to geochronology. Geochim. Cosmochim. Acta 50, 2855–2862.
Kurz, M.D., Brook, E.J., 1994. Surface exposure dating with cosmogenic nuclides. In: Beck, C. (Ed.), Dating in Exposed and Surface Contexts. University of New Mexico Press, pp. 139–159.
Kurz, M.D., Geist, D., 1999. Dynamics of the Galapagos hotspot from helium isotope geochemistry. Geoch. Cosmochim. Acta 63, 4139–4156.
Lal, D., 1991. Cosmic ray labelling of erosion surfaces: in situ nuclide production rates and erosion models. Earth Plan. Sci. Lett. 104, 424–439.
Licciardi, J.M., Kurz, M.D., Clark, P.U., Brook, E.J., 1999. Calibration of cosmogenic ^{3}He production rates from Holocene lava flows in Oregon, USA, and effects of the Earth's magnetic field. Earth Plan. Sci. Lett. 172, 261–271.
Licciardi, J.M., Clark, P.U., Brook, E.J., Pierce, K.L., Kurz, M.D., Elmore, D., Sharma, P., 2001. Cosmogenic ^{3}He and ^{10}Be chronologies of the late Pinedale northern Yellowstone ice cap, Montana, USA. Geology 29, 1095–1098.
Margerison, H.R., Phillips, W.M., Stuart, F.M., Sugden, D.E., 2005. Cosmogenic ^{3}He concentrations in ancient flood deposits from the Coombs Hills, northern Dry Valleys, East Antarctica: interpreting exposure ages and erosion rates. Earth Plan. Sci. Lett. 230, 163–175.
Min, K., Reiner, P.W., Wolff, J.A., Mundil, R., Winters, R.L., 2006. (U–Th)/He dating of volcanic phenocrysts with high-U–Th inclusions, Jemez volcanic field, New Mexico. Chem. Geol. 227, 223–235.
Schäfer, J.M., Ivy-Ochs, S., Wieler, R., Leya, I., Baur, H., Denton, G.H., Schlücter, C., 1999. Cosmogenic noble gas studies in the oldest landscape on earth: surface exposure ages of the Dry Valleys, Antarctica. Earth Plan. Sci. Lett. 167, 215–226.
Schäfer, J.M., Baur, H., Denton, G.H., Ivy-Ochs, S., Marchant, D.R., Schlücter, C., Weiler, R., 2000. The oldest ice on Earth in Beacon Valley, Antarctica: new evidence from surface exposure dating. Earth Plan. Sci. Lett. 179, 91–99.
Van der Wateren, F.M., Dunai, T.J., Van Balen, R.T., Klas, W., Verbers, A.L.L.M., Passchier, S., Herpers, U., 1999. Contrasting neogene denudation histories of different structural regions in the Transantarctic Mountains rift flank constrained by cosmogenic isotope measurements. Glob. Planet. Change 23, 145–172.
Venturelli, G., Fragipane, M., Weibel, M., Antiga, D., 1978. Trace element distribution in the Cainozoic lavas of Nevado Coropuna and Andagua Valley, Central Andes of southern Peru. Bull. Volcanol. 41, 213–228.